DECEMBER 2009 VOL 4 NO 12
www.nature.com/naturenanotechnology

nature nanotechnology

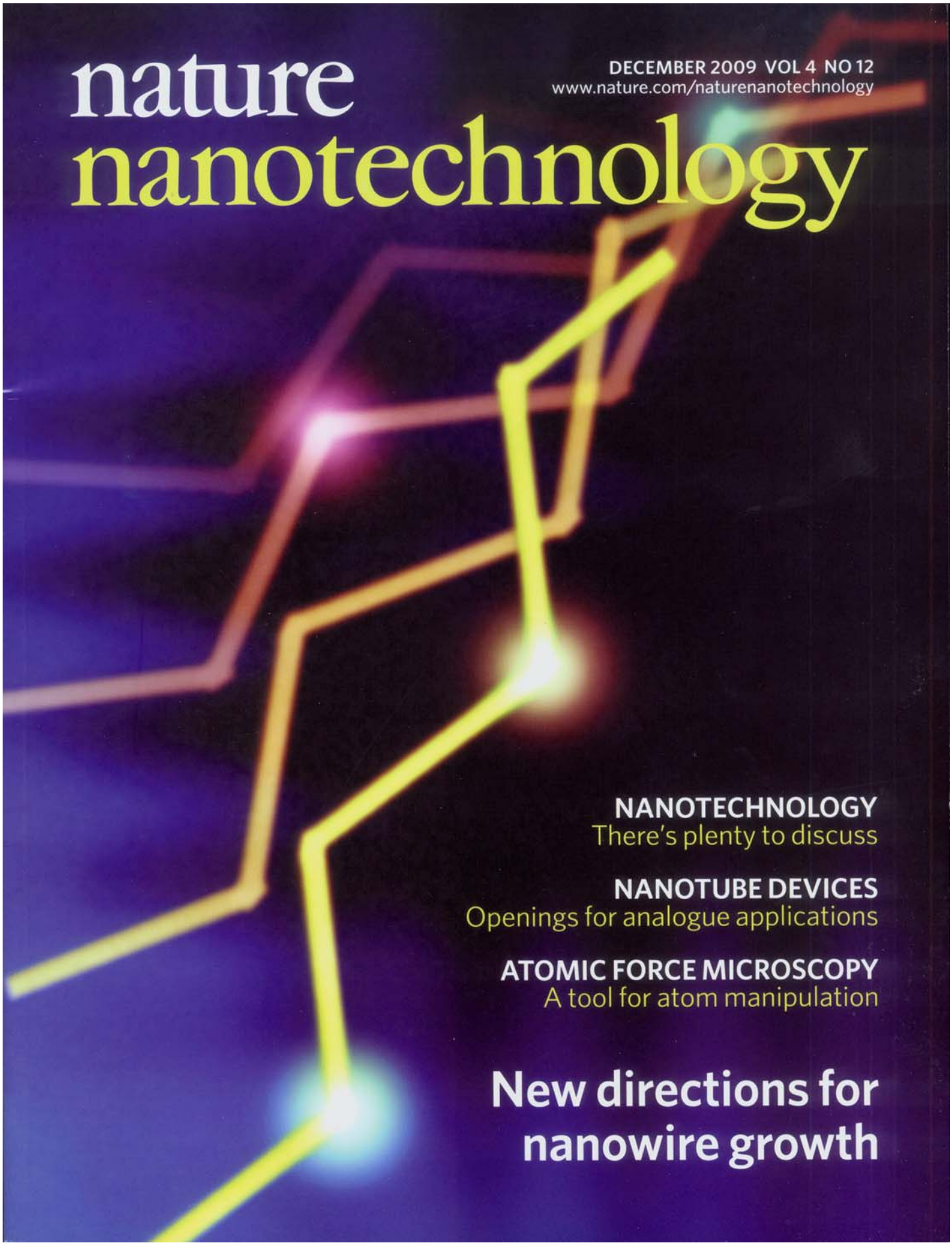

NANOTECHNOLOGY
There's plenty to discuss

NANOTUBE DEVICES
Openings for analogue applications

ATOMIC FORCE MICROSCOPY
A tool for atom manipulation

New directions for nanowire growth

LETTERS
PUBLISHED ONLINE: 18 OCTOBER 2009 | DOI: 10.1038/NNANO.2009.304
nature nanotechnology

Single-crystalline kinked semiconductor nanowire superstructures

Bozhi Tian[1], Ping Xie[1], Thomas J. Kempa[1], David C. Bell[2] and Charles M. Lieber[1,3]*

The ability to control and modulate the composition[1–4], doping[1,3–5], crystal structure[6–8] and morphology[9,10] of semiconductor nanowires during the synthesis process has allowed researchers to explore various applications of nanowires[11–15]. However, despite advances in nanowire synthesis, progress towards the *ab initio* design and growth of hierarchical nanostructures has been limited. Here, we demonstrate a 'nanotectonic' approach that provides iterative control over the nucleation and growth of nanowires, and use it to grow kinked or zigzag nanowires in which the straight sections are separated by triangular joints. Moreover, the lengths of the straight sections can be controlled and the growth direction remains coherent along the nanowire. We also grow dopant-modulated structures in which specific device functions, including p–n diodes and field-effect transistors, can be precisely localized at the kinked junctions in the nanowires.

We have focused on the rational design and synthesis of two-dimensional multiply kinked nanowires (Fig. 1a), in which kinks are introduced at defined positions during growth and are confined to a single plane. These hierarchical nanowires are constructed using a nanotectonic approach analogous to metal–organic framework materials[16], where we define a secondary building unit (SBU)[16] consisting of two straight single-crystalline arms (blue, Fig. 1a) connected by one fixed 120° angle joint (green, Fig. 1a). Note that two $\langle 112\rangle_c$ or $\langle 110\rangle_c$ vectors in a cubic crystal structure and two $\langle 11\text{–}20\rangle_h$ or $\langle 1\text{–}100\rangle_h$ vectors in a hexagonal structure can form the desired 120° joint when rotating about the $\langle 111\rangle_c$ and $\langle 0001\rangle_h$ zone axes, respectively (Fig. 1a; Supplementary Fig. S1). SBU formation involves three main steps during nanocluster-catalysed growth (Fig. 1b); (1) axial growth of a one-dimensional nanowire arm segment, (2) purging of gaseous reactants to suspend nanowire elongation, and (3) supersaturation and nucleation of nanowire growth following re-introduction of reactants. As illustrated for the case of silicon, the concentration of silicon-reactant dissolved in the nanocluster catalyst drops during purging and then reaches a maximum upon supersaturation. Steps (1) to (3) can be iterated to link a number of SBUs, generating a two-dimensional chain structure.

We first illustrate this approach with the synthesis of two-dimensional silicon nanowire chains. We synthesized ~80-nm-diameter silicon nanowires with dominant $\langle 112\rangle$ axial orientation using a gold nanocluster-catalysed vapour–liquid–solid (VLS) method[17–19] (see Methods and Supplementary Fig. S2). Scanning electron microscopy (SEM) images of a typical kinked silicon nanowire structure (Fig. 1c), produced by iterating the (1) to (3) cycle several time so as to yield equal-length segments, highlight several notable features. First, well-defined two-dimensional kinked nanowire structures are observed that have equal arm lengths, consistent with the constant segment growth times, and uniform diameters. Second, the clearly visible gold catalyst at the nanowire tip (Fig. 1c,d) and uniform diameter indicate that growth proceeds by means of the nanocluster-catalysed VLS process[17–19] throughout the whole synthesis process. Third, the joint angle is a constant 120° and all SBUs are confined in a single two-dimensional plane consistent with our model (Fig. 1a). Finally, the yield of such a kinked two-dimensional chain structure is greater than 40% for these 80-nm-diameter nanowires with purge times (step (2)) of 15 s (Supplementary Fig. S3), the remaining nanowires having a one-dimensional morphology. The kinked nanowire structures could be purified to further enhance yields, and we note that the simple dispersion and deposition process used to prepare samples for analysis leads to a preferential enhancement of the yield on substrates.

To address the potential of *ab initio* design and synthesis we have prepared kinked silicon nanowires in which the arm length is intentionally varied. A representative SEM image of a structure with six distinct segment lengths (Fig. 1d) reveals that the formation of well-defined SBU kinks is independent of the constituent segment lengths within a range of at least 180–2,500 nm as investigated. Analysis of the segment lengths in uniformly kinked nanowire samples yields a linear dependence of segment length on axial growth time (Fig. 1e), further supporting our demonstration of well-controlled VLS growth. The slope of the linear fit yields a nanowire axial growth rate of 870 nm min^{-1} at constant pressure and uniform flow (Fig. 1e inset and Methods). The differential segment length data extracted from Fig. 1d are also plotted (magenta squares); these agree very well with the data acquired from the kinked nanowires with uniform segments, demonstrating a high level of control for independent syntheses and, correspondingly, the capability for *ab initio* design and synthesis. Note also that these results, which show that segment length is fully determined by growth time, are distinct from the self-organized growth models used to explain oscillatory sawtooth faceting in nonpolar silicon nanowires[9] or twinning superlattices in $\langle 111\rangle$ B-oriented III–V nanowires[6–8].

We have also determined the atomic-level structure of the two-dimensional kinked nanowires using transmission electron microscopy (TEM). A representative TEM image (Fig. 2a) of a multiply kinked silicon nanowire, and selected area electron diffraction (SAED) patterns recorded from non-adjacent joints (Fig. 2b), show that the entire nanostructure is single crystalline and that the arms and joints are free of bulk dislocations and defects. The SAED patterns from kink positions I and II, which are separated by ~3 μm and two intervening kinks, can be indexed for the $\langle 111\rangle$ zone axis and show that the two-dimensional chain structure extends in the $\{111\}$ plane and that the segments grow along the $\langle 112\rangle$ direction in a coherent manner. These observations are consistent with our orientation-controlled nanowire growth and SBU model (Fig. 1a).

TEM images of a single kink (Fig. 2c,d) further illustrate key SBU features. The images demonstrate that there are no atomic-scale

[1]Department of Chemistry and Chemical Biology, Harvard University, Cambridge, Massachusetts 02138, USA, [2]Center for Nanoscale Systems, Harvard University, Cambridge, Massachusetts 02138, USA, [3]School of Engineering and Applied Sciences, Harvard University, Cambridge, Massachusetts 02138, USA. *e-mail: cml@cmliris.harvard.edu

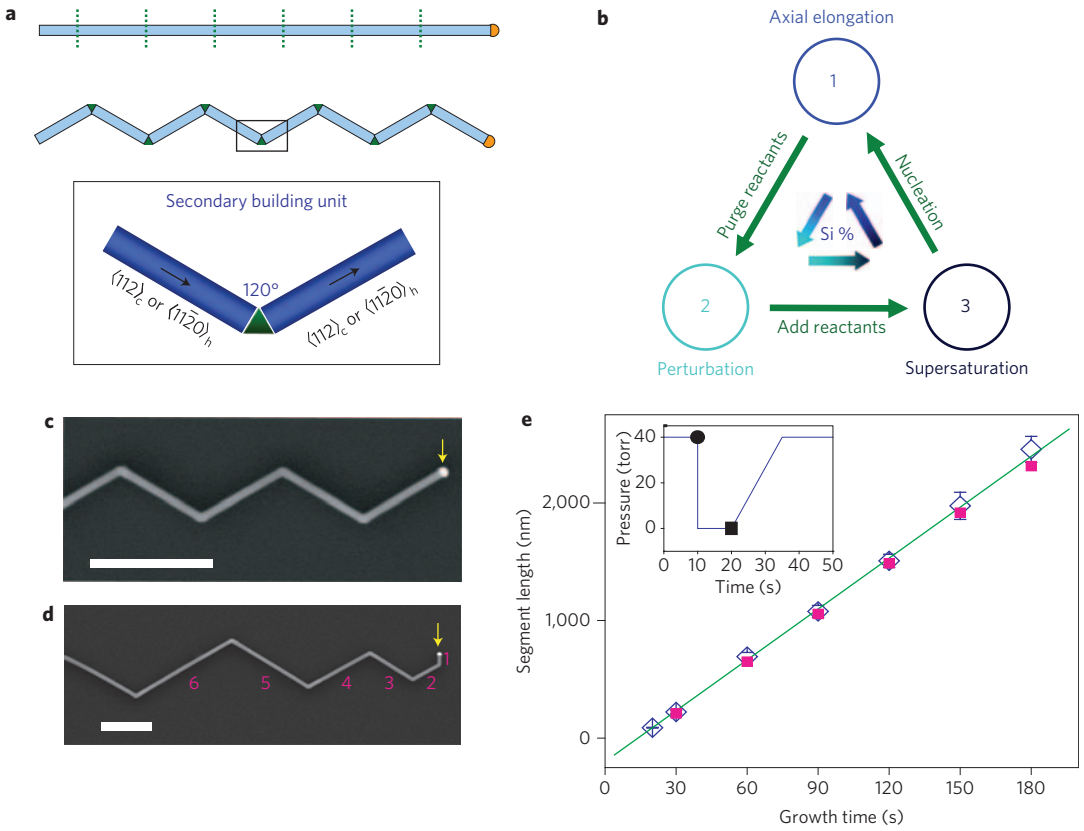

Figure 1 | Design and controlled synthesis of multiply kinked nanowires. a, Schematic of a coherently kinked nanowire and the secondary building unit (SBU), which contains two arms (blue) and one joint (green). The multiply kinked nanowires (middle panel) are derived from the corresponding one-dimensional nanowire by introducing the joints at the points indicated by the dashed lines in the upper panel. Subscripts c and h denote cubic and hexagonal structures, respectively. **b**, Cycle for the introduction of a SBU by stepwise synthesis. The colour gradient accompanying the innermost blue arrows indicates the change of silicon concentration in nanocluster catalyst during synthesis of a kinked silicon nanowire. **c**, SEM image of a multiply kinked two-dimensional silicon nanowire with equal arm segment lengths. Scale bar, 1 μm. The yellow arrow highlights the position of the nanocluster catalyst. **d**, SEM image of a multiply kinked silicon nanowire with decreasing arm segment lengths. Scale bar, 1 μm. The growth durations are 30, 60, 90, 120, 150 and 180 s for segments 1 to 6, respectively. The yellow arrow highlights the position of the nanocluster catalyst. SEM images shown in **c** and **d** were acquired without substrate tilting, and the electron beam perpendicular to the two-dimensional plane of the multiply kinked nanowires. **e**, Plot of segment length versus growth time. Each blue diamond represents average segment length data (error bars: ±1 s.d.) from a sample containing nanowires with uniform segment lengths between kinks. The green line is a linear fit to these data. Magenta solid squares are data points taken from the nanowire shown in **d**. Inset, growth pressure variation during kink synthesis. The black solid sphere and square denote the start of purging and re-introduction of reactants, respectively.

twin defects or stacking faults, confirming a single-crystal structure across the complete arm–joint–arm junction. This is distinct from other recent reports of modulated nanowires such as twinning superlattices[6–8] that comprised twin planes and/or stacking faults. Furthermore, the SBU reported in our work is unique in that it preserves crystallographic orientation and composition in arms over multiple kinks, in contrast to single kinks observed previously[20,21], where the arms had either different growth directions[20] or compositions[21]. Second, the joint has a quasi-triangular structure with {111} top/bottom facets and two {112} side facets joining the adjacent arms. Finally, the nanowire growth direction changes during growth of the kink, following $\langle 112\rangle_{arm}$ to $\langle 110\rangle_{joint}$ to $\langle 112\rangle_{arm}$.

To shed light on the mechanism and limits of the single-crystalline kinked junction formation, we characterized the kink frequency as a function of key parameters, including nanowire diameter and purge time. The kink frequency is defined as $P_{kink} = N_k/N_t = N_k/(N_k + N_s)$, where N_t, N_k and N_s denote the number of total designed junctions, observed kink junctions, and observed straight and node-like junctions, respectively. Under optimal growth conditions (see Methods), both 80- and 150-nm silicon nanowires (Fig. 3a) show a high probability of kinks with a regular zigzag geometry. When the purge time of step B (Fig. 1b) is reduced from optimal to 3 or 1 s, nodes or incipient kinks (Fig. 3b) are observed at the positions expected for kinks based on elongation time and growth rate. Higher resolution SEM or TEM images define the nodes as regions of slightly larger diameter with lengths of ~50 nm. A summary of results for 80- and 150-nm diameters obtained for 1, 3 and 15 s purges (Fig. 3c) quantifies these observations and shows that this reduced kink frequency with decreasing purge times is more pronounced in nanowire samples with larger diameters. These results are consistent with the reactant concentration drop from the nanocluster catalyst being critical for kink formation because the relative concentration drop will be smaller at a fixed purge time in larger versus smaller diameter nanowires[22].

Overall, the above studies suggest kink formation can be qualitatively explained by the proposed stepwise model shown in Fig. 3d. In step 1, the reactant concentration drops in the supersaturated catalyst during the purge, and if the concentration is reduced sufficiently, elongation will cease. When reactant is re-introduced in step 2, the catalyst can become supersaturated again and undergo heterogeneous nucleation[23,24] and growth. For short purge times and nanowires with larger diameter, the reactant concentration is sufficient for elongation to continue; however, as shown in *in situ* TEM studies[22], this situation can lead to a flattening of the catalyst

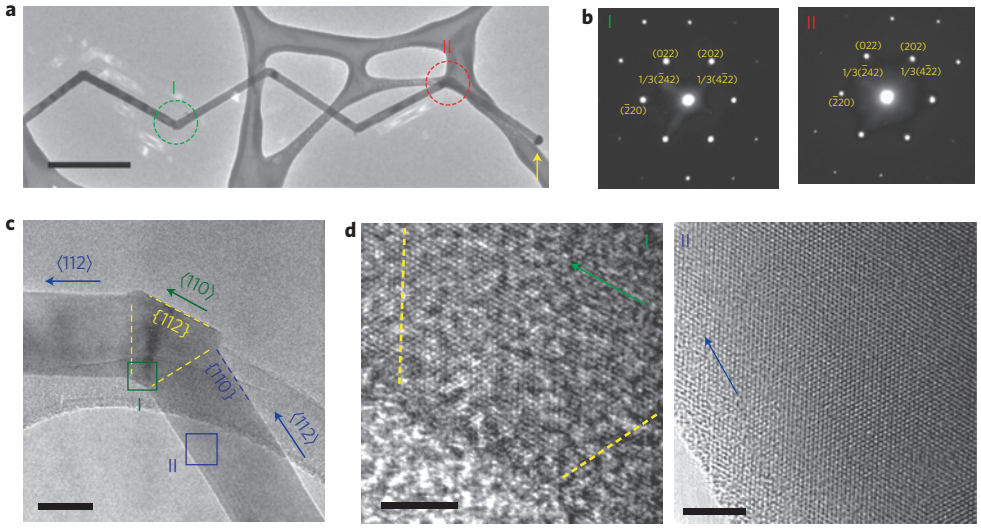

Figure 2 | Crystallographic structure of kinked silicon nanowires. a, Bright-field TEM image of a multiply kinked silicon nanowire. Scale bar, 1 μm. The green (region I) and red (region II) dashed circles highlight non-adjacent kinks where diffraction data were recorded. The yellow arrow highlights the position of the nanocluster catalyst. **b**, SAED patterns recorded from regions I and II in **a**. The SAED patterns were recorded along the ⟨111⟩ zone axis. **c**, TEM image of a single kink with crystallographic directions and facets indicated by arrows and dashed lines, respectively. Scale bar, 50 nm. The green (region I) and blue (region II) open squares highlight regions of the joint and one arm where high-resolution images were recorded. **d**, Lattice-resolved TEM images from regions **I** and **II** in **c**. Scale bars, 5 nm. Dashed lines and arrows denote crystallographic planes and growth directions, respectively. All TEM images and SAED patterns were acquired with the electron beam perpendicular to the two-dimensional plane of the kinked nanowires.

nanodroplet and an increase in nanowire diameter consistent with the formation of nodes (Fig. 3b, marked with blue stars). In step 3, growth proceeds with preservation of the most stable {111} facets[25], thus implying that the heterogeneous nucleation should occur preferentially at the active {110} edges[26] of the three-phase boundary[24]. This model yields a transition from the ⟨112⟩ to ⟨110⟩ direction about the ⟨111⟩ axis. This growth along ⟨110⟩ is transient because this direction is not thermodynamically favourable in this diameter regime[19,20] (Supplementary Fig. S2), and in step 4, the kink is completed with a transition to another ⟨112⟩ direction, thus completing a single SBU with coherent arm growth directions. We did not observe ⟨112⟩ to ⟨111⟩ growth switching[20] in our kinked structures, most probably because the growth of a ⟨111⟩ segment requires the formation of six new {112} facets[9] and the disappearance of two stable {111} facets[26] of the initial ⟨112⟩ segment.

Although additional experiments will be necessary to clarify details of the kink formation hypothesis in our proposed growth model, we note that this model now enables the design and synthesis of specific structures in silicon nanowires and, more generally, nanowire systems with distinct compositions. To illustrate this point, we first designed and synthesized $(\text{kink-node})_m$ and $(\text{kink-node})_m(\text{kink})_n$ modulated silicon nanowire structures, where m and n are indices denoting the number of times the growth of the structural unit is repeated. We chose 150-nm gold as the catalysts, and 15 and 1 s as the purge durations (Fig. 3c) for the growth of kinks and nodes, respectively. Notably, SEM images of the $(\text{kink-node})_m$ structure (Fig. 3e, I and II) show that the nodes (highlighted with yellow stars) are reproducibly inserted between kinks over multiple modulations. These results also show that the formation of individual kinks or nodes is independent of adjacent elements and is controlled by growth conditions. This latter point and possible control is further demonstrated by the synthesis of coherent $(\text{kink})_8$ SBUs following modulated $(\text{kink-node})_4$ units (Fig. 3e, III). Interestingly, the observation of coherent zigzag chain structures suggests that 'steering' of kinks is not random and might be due, for example, to a minimization of stress or maintenance of the centre-of-mass of the whole structure. Although further studies will be required to understand coherence in multiply kinked structures, we believe that these results already highlight an emerging potential of our nanotectonic approach to generate, in a predictable manner, complex two-dimensional nanowire structures.

Furthermore, we have used our model for the designed synthesis of two-dimensional kinked nanowire structures in other materials. For example, SEM images (Fig. 4a) of germanium nanowires grown using the iterative approach of Fig. 1a (see Methods) show nanowires with well-defined kinks, where the kink angle, 120°, is consistent with that for the SBU. TEM images (Fig. 4b) further demonstrate that (i) the growth direction of the arms of the two-dimensional kinked germanium nanowires are along the ⟨112⟩ direction and (ii) the joint is single-crystalline. These structural details are consistent with the general features observed in kinked silicon nanowires (Figs 1 and 2). Our model also predicts that the arm–joint–arm kink SBU could be realized in very different materials such as the wurtzite phase of the group II–VI semiconductor CdS. Notably, designed iterative modulation of the growth of ⟨11–20⟩ direction CdS nanowires yields a regular two-dimensional kinked structure with 120° kink angle as shown in Fig. 4c. TEM images (Fig. 4d) demonstrate that the CdS two-dimensional kinked nanowire structure is single-crystalline, with arms all along the ⟨11–20⟩ direction of the wurtzite phase. Finally, we suggest our approach could also be used for the designed synthesis of two-dimensional kinked group III–V nanowire materials such as GaN nanowires, which have been reported with almost pure ⟨11–20⟩ orientation[4].

These results highlight an emerging potential for our bottom-up nanotectonic approach to generate more complex nanowires with potentially unique function integrated at the nanoscale in the topologically defined points of the kinks. We illustrate this capability by combining our iterative growth approach with additional modulation of the dopant to vary the electronic characteristics in a well-defined manner with respect to the kinks. A kinked silicon nanowire SBU with integrated n- and p-type arms was synthesized by switching phosphine and diborane dopants during the kink growth sequence (see Methods). Current–voltage (I–V) data recorded on a representative single kink device (Fig. 5a) reveal a clear current rectification in reverse bias with an onset at a forward bias voltage of ~0.6 V, consistent with the synthesis of a well-defined p–n diode within the kinked structure. Moreover,

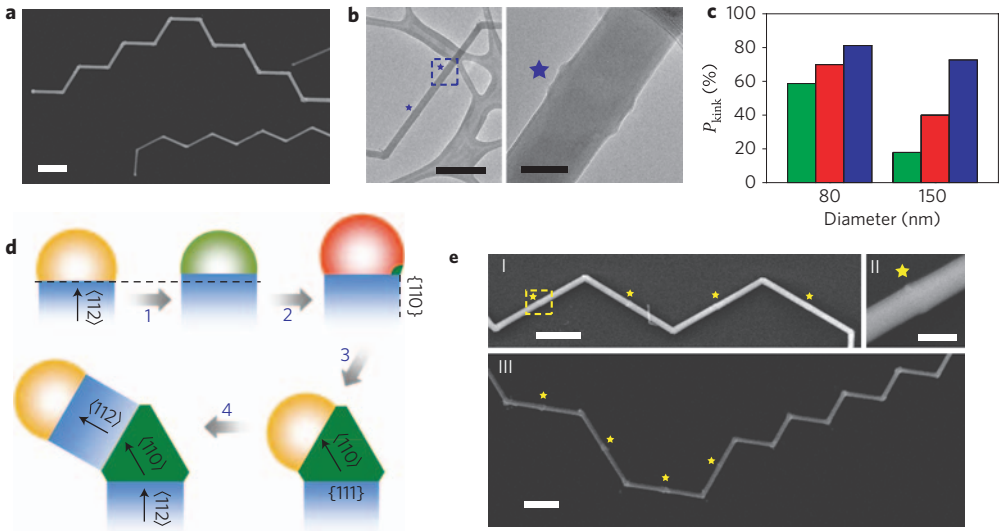

Figure 3 | Mechanistic studies of kinked nanowire growth. a, SEM images of 150- (upper) and 80-nm (lower) diameter kinked silicon nanowires grown with periodic 15 s purges. Scale bar, 1 μm. **b**, TEM images at low (left panel) and high (right panel) magnification of one 80-nm-diameter silicon nanowire segment subjected to a 1 s purge. The blue stars mark incipient kinks or nodes, and the dashed square corresponds to the region where the right panel was recorded. Scale bars, 500 (left) and 50 nm (right). **c**, Kink frequency (P_{kink}) histogram for 80- and 150-nm diameter silicon nanowires grown with different purge durations. Green, red and blue bars denote results from 1, 3 and 15 s purges, respectively, and are averaged over at least 15 multiply kinked nanowires. **d**, Schematic illustrating the key stages of kink formation. Arrows 1–4 denote purge, re-introduction of reactant, joint growth and subsequent arm growth, respectively. **e**, SEM images of two-dimensional silicon nanowires with modulated kinks and incipient kinks (starred nodes). I corresponds to a designed $(kink\text{-}node)_m$ structure; II is an enlargement of one node from the region indicated by the dashed yellow square in I; and III corresponds to a $(kink\text{-}node)_m(kink)_n$ structure, where *m and n* are integers. The angle between the norm of the kinked nanowire plane and the electron beam in III is ~50°. All other images were acquired with the electron beam perpendicular to the two-dimensional plane of the kinked nanowires. Scale bars in I, II and III are 1, 0.2 and 1 μm, respectively.

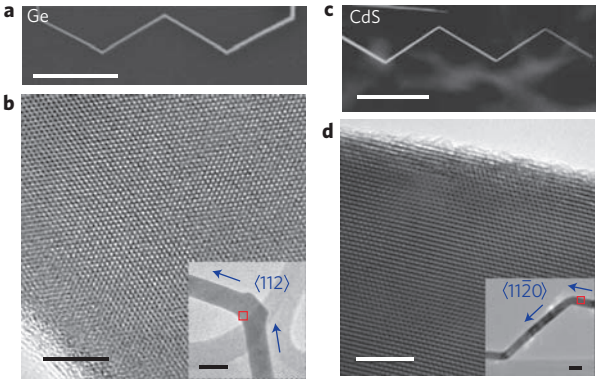

Figure 4 | Generality of kinked nanowire synthesis. a, SEM image of one multiply kinked germanium nanowire. Scale bar, 1 μm. **b**, Lattice-resolved TEM image of the joint region of a representative germanium nanowire kink. Scale bar, 5 nm. Inset highlights one secondary building unit (SBU) with arrows corresponding to ⟨112⟩ growth directions and the red square to the region where the high-resolution image was recorded. Inset scale bar, 50 nm. **c**, SEM image of one multiply kinked CdS nanowire. Scale bar, 1 μm. **d**, Lattice-resolved TEM image of the arm region of a representative CdS adjacent to the kink joint. Scale bar, 5 nm. The inset highlights two SBUs with the arrows corresponding to the ⟨11–20⟩ growth directions and the red square to the region where the high-resolution image was recorded. Inset scale bar, 50 nm. All images were acquired with the electron beam perpendicular to the two-dimensional plane of the kinked nanowires.

an electrostatic force microscopy (EFM) image of a typical kinked p–n nanowire in reverse bias (Fig. 5b) showed that the voltage drop occurs primarily at the designed p–n junction localized and labelled by the kink during growth.

Furthermore, our concept can be extended to the design and synthesis of nanowires with distinct functionality at sequential kinks. A representative atomic force microscopy (AFM) image of a double kink structure synthesized with n^+ and n dopant profiles at the two kink joints (Fig. 5c) shows that the characteristic SBU described above is unaffected by multiple modulations of dopant concentration. Notably, scanned gate microscopy (SGM) data (Fig. 5d) demonstrate enhanced (decreased) nanowire conductance as the tip with positive (negative) gate potential is scanned across the designed n-type segment immediately adjacent to the upper-left kink junction, thus confirming the integration of an n-type field-effect transistor at a well-defined and recognizable point on the structure. The absence of gate response from the lower-right kink junction (Fig. 5d) further shows that the single-crystalline kink structure itself will not alter the electrical transport properties. We believe that these synthetic results and demonstrated topologically defined functional devices represent a significant advance towards the realization of *ab initio* designed and 'self-labelled' two-dimensional nanowire structures. Such designed and self-labelled two-dimensional nanowire structures may open up unique applications in the bottom-up integration of active devices in nanoelectronics, photodetector arrays, multiplexed biological sensors and the development of multi-terminal nanodevices in three dimensions.

Methods

Nanowire synthesis. Single-crystalline kinked nanowires were synthesized using the nanocluster-catalysed VLS method described previously[18,19] in a quartz tube connected to a gas manifold and vacuum pump and heated by a temperature-controlled tube furnace. Monodisperse gold nanoparticles (Ted Pella) were dispersed on SiO_2/silicon or sapphire growth substrates (gold surface coverage: 0.01–0.1 particles μm^{-2}), which were placed within the central region of the quartz tube reactor. Nanowires grown on both substrates yielded similar kink morphologies and yields. The silicon nanowires were synthesized at 450–460°C using silane (SiH_4) as the silicon reactant source, H_2 as the carrier gas, and phosphine (PH_3, 1,000 ppm in H_2) and diborane (B_2H_6, 100 ppm in H_2) as the n- and p-type dopants. In a typical

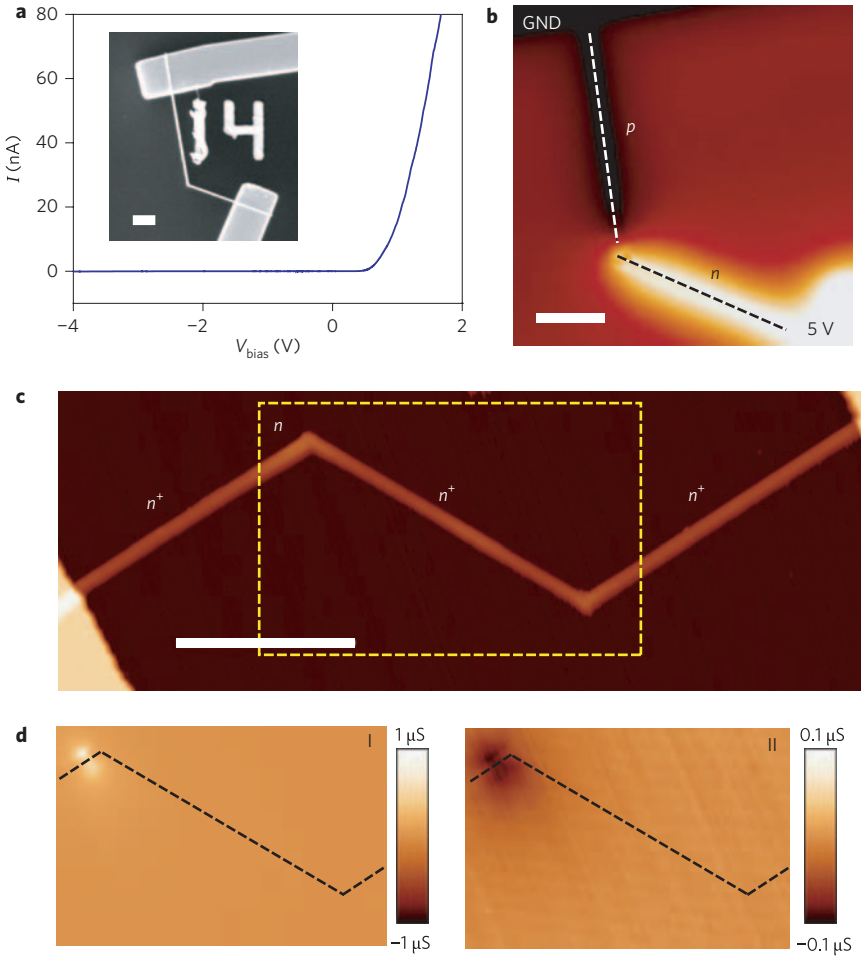

Figure 5 | Topologically defined nanoelectronic devices. a, *I*–*V* data recorded from a kinked p–n silicon nanowire device. Inset: SEM image of the device structure. Scale bar, 2 μm. **b**, EFM image of a p–n diode reverse-biased at 5 V. The AFM tip voltage was modulated by 3 V at the cantilever-tip resonance frequency. The signal brightness is proportional to the nanowire device surface potential, and shows an abrupt drop around the kink position. The dashed lines mark the nanowire position. Scale bar, 2 μm. **c**,**d**, AFM and SGM images of one n^+−kink−n^+−kink−(n−n^+) dopant modulated double-kinked silicon nanowire structure. Scale bar in **c**, 2 μm. The SGM images were recorded with a V_{tip} of 10 V (I) and −10 V (II), respectively, and V_{sd} of 1 V. The dark and bright regions correspond to reduced and enhanced conductance, respectively. The black dashed lines mark the nanowire position.

synthesis of uniform n-type, 80-nm kinked silicon nanowires, the flow rates of SiH_4, PH_3 and H_2 were 1–2, 2–10 and 60 standard cubic centimetres per minute, respectively, and the total pressure 40 torr and purge duration 10–15 s; the minimum pressure during the purge cycle was $\sim 3 \times 10^{-3}$ torr. The dopant feed-in ratios (silicon:boron/phosphorus) in kinked p–n silicon nanowires were 500:1 for both p- and n-type segments. In n^+–kink–n^+–kink–(n–n^+) dopant modulated silicon nanowires, the silicon–phosphorus feed-in ratios were 200:1 and 10,000:1 for n^+- and n-type segments, respectively, and the n-type segment was grown for 30 s. Germanium nanowires were synthesized at 270–290 °C, 40 torr, with germane (GeH_4, 10% in H_2) and H_2 as the reactant and carrier gas, respectively. CdS nanowires were grown in a three-zone furnace by evaporating CdS power at 650–720 °C, with nanowire growth using gold nanocluster-catalysed VLS method at 550–500 °C. The purge cycle used to form kinks in the germanium and CdS nanowires was typically 15 s.

Structure characterization. Zeiss Ultra55/Supra55VP field-emission SEMs and a JEOL 2010 field-emission TEM were used to carry out SEM and TEM analyses, respectively. For sample preparation, kinked nanowires were gently sonicated in isopropyl alcohol and dispersed onto heavily doped silicon substrates (100-nm oxide/200-nm nitride; resistivity, 1–10 Ω cm, Nova Electronic Materials) or lacey carbon grids (Ted Pella).

Device fabrication and measurement. Devices were fabricated on silicon substrates (Nova Electronic Materials, n-type 0.005 Ω cm) with 100-nm thermal oxide and 200-nm SiN at the surface. Devices were defined by electron-beam lithography followed by titanium/palladium (1.5 nm/100 nm) contact deposition in a thermal evaporator. Current–voltage (*I*–*V*) data were recorded using an Agilent semiconductor parameter analyser (Model 4156C) with contacts to devices made using a probe station (Desert Cryogenics, Model TTP4). EFM and SGM measurements were carried out with a Digital Instruments Nanoscope IIIa MultiMode AFM and metal-coated tips (Nanosensors, PPP-NCHPt). The EFM surface potential maps and SGM conductance maps were acquired in lift mode with lift heights of 40 and 20 nm, respectively. In the surface potential measurements, the p–n diode was reverse-biased at 5 V and the tip voltage was modulated by 3 V at the resonance frequency. In SGM measurements, the tip functions as a local gate $V_{tip} = \pm 10$ V, and the conductance versus position provides a measure of local accumulation or depletion of carriers in the device.

Received 2 June 2009; accepted 15 September 2009; published online 18 October 2009

References

1. Gudiksen, M. S., Lauhon, L. J., Wang, J., Smith, D. C. & Lieber, C. M. Growth of nanowire superlattice structures for nanoscale photonics and electronics. *Nature* **415,** 617–620 (2002).
2. Bjork, M. T. *et al.* One-dimensional heterostructures in semiconductor nanowhiskers. *Appl. Phys. Lett.* **80,** 1058–1060 (2002).
3. Lauhon, L. J., Gudiksen, M. S., Wang, D. L. & Lieber, C. M. Epitaxial core–shell and core–multishell nanowire heterostructures. *Nature* **420,** 57–61 (2002).
4. Qian, F., Li, Y., Gradečak, S., Wang, D. L., Barrelet, C. J. & Lieber, C. M. Gallium nitride-based nanowire radial heterostructures for nanophotonics. *Nano Lett.* **4,** 1975–1979 (2004).
5. Yang, C., Zhong, Z. H. & Lieber, C. M. Encoding electronic properties by synthesis of axial modulation-doped silicon nanowires. *Science* **310,** 1304–1307 (2005).
6. Algra, R. E. *et al.* Twinning superlattices in indium phosphide nanowires. *Nature* **456,** 369–372 (2008).

7. Caroff, P. *et al.* Controlled polytypic and twin-plane superlattices in III–V nanowires. *Nature Nanotech* **4,** 50–55 (2009).
8. Davidson, F. M., Lee, D. C., Fanfair, D. D. & Korgel B. A. Lamellar twinning in semiconductor nanowires. *J. Phys. Chem. C* **111,** 2929–2935 (2007).
9. Ross, F. M., Tersoff, J. & Reuter, M. C. Sawtooth faceting in silicon nanowires. *Phys. Rev. Lett.* **95,** 146104 (2005).
10. Gao, P. X. *et al.* Conversion of zinc oxide nanobelts into superlattice-structured nanohelices. *Science* **309,** 1700–1704 (2005).
11. Lu, W. & Lieber, C. M. Nanoelectronics from the bottom up. *Nature Mater.* **6,** 841–850 (2007).
12. Sirbuly, D. J., Law, M., Yan, H. Q. & Yang, P. D. Semiconductor nanowires for subwavelength photonics integration. *J. Phys. Chem. B* **109,** 15190–15213 (2005).
13. Patolsky, F., Timko, B. P., Zheng, G. & Lieber, C. M. Nanowire-based nanoelectronic devices in the life sciences. *MRS Bull.* **32,** 142–149 (2007).
14. Stern, E. *et al.* Label-free immunodetection with CMOS-compatible semiconducting nanowires. *Nature* **7127,** 519–522 (2007).
15. McAlpine, M. C., Ahmad, H., Wang, D. W. & Heath, J. R. Highly ordered nanowire arrays on plastic substrates for ultrasensitive flexible chemical sensors. *Nature Mater.* **6,** 379–384 (2007).
16. Yaghi, O. M. *et al.* Reticular synthesis and the design of new materials. *Nature* **423,** 705–714 (2003).
17. Wagner, R. S. & Ellis, W. C. Vapor–liquid–solid mechanism of single crystal growth. *Appl. Phys. Lett.* **4,** 89–90 (1964).
18. Morales, A. M. & Lieber, C. M. A laser ablation method for the synthesis of crystalline semiconductor nanowires. *Science* **279,** 208–211 (1998).
19. Wu, Y. *et al.* Controlled growth and structures of molecular-scale silicon nanowires. *Nano Lett.* **4,** 433–436 (2004).
20. Lugstein, A. *et al.* Pressure-induced orientation control of the growth of epitaxial silicon nanowires. *Nano Lett.* **8,** 2310–2314 (2008).
21. Dick, K. A. *et al.* The morphology of axial and branched nanowire heterostructures. *Nano Lett.* **7,** 1817–1822 (2007).
22. Kodambaka, S., Tersoff, J., Reuter, M. C. & Ross, F. M. Germanium nanowire growth below the eutectic temperature. *Science* **316,** 729–732 (2007).
23. Kim, B. J. *et al.* Kinetics of individual nucleation events observed in nanoscale vapor–liquid–solid growth. *Science* **322,** 1070–1073 (2008).
24. Wacaser, B. A. *et al.* Preferential interface nucleation: an expansion of the VLS growth mechanism for nanowires. *Adv. Mater.* **21,** 153–165 (2009).
25. Jaccodine, R. J. Surface energy of germanium and silicon. *J. Electrochem. Soc.* **110,** 524–527 (1963).
26. Pan, L., Lew, K.-K., Redwing, J. M. & Dickey, E. C. Stranski–Krastanow growth of germanium on silicon nanowires. *Nano Lett.* **5,** 1081–1085 (2005).

Acknowledgements

The authors would like to thank Y. J. Dong, X. C. Jiang and Q. Qing for help with experiments. C.M.L. acknowledges support from a National Institutes of Health Director's Pioneer Award, a McKnight Foundation Neuroscience Award and a contract from MITRE Corporation. T.J.K acknowledges support from the National Science Foundation Graduate Research Fellowship.

Author contributions

B.T. and C.M.L. designed the experiments. B.T., P.X. and T.J.K. performed experiments and analyses. B.T. and C.M.L. co-wrote the paper. All authors discussed the results and commented on the manuscript.

Additional information

Supplementary information accompanies this paper at www.nature.com/naturenanotechnology. Reprints and permission information is available online at http://npg.nature.com/reprintsandpermissions/. Correspondence and requests for materials should be addressed to C.M.L.